J Nanopart Res (2013) 15:2092
DOI 10.1007/s11051-013-2092-5

RESEARCH PAPER

Starch-modified magnetite nanoparticles for impregnation into cartilage

Yulia M. Soshnikova · Svetlana G. Roman · Natalia A. Chebotareva · Olga I. Baum · Mariya V. Obrezkova · Richard B. Gillis · Stephen E. Harding · Emil N. Sobol · Valeriy V. Lunin

Received: 5 May 2013 / Accepted: 19 October 2013 / Published online: 1 November 2013

Abstract The paper presents preparation and characterization of starch-modified Fe_3O_4 nanoparticles (NPs) in aqueous dispersion after impregnation into healthy and damaged types of cartilage. We show that starch-modified dispersion has a narrower size distribution than a non-stabilized one. The average hydrodynamic radius of magnetite NPs in a dispersion used for impregnation into cartilage is (48 ± 1) nm with the width of the distribution from 5 to 200 nm. We investigate stability of aqueous magnetite NPs dispersions during storage and with increase in temperature (up to 70 °C). We find that polydisperse magnetite NPs can penetrate into cartilage and the size and concentration of impregnated particles depend on the organization of the tissue structure. The results confirm the possibility of application of magnetite NPs in diagnostics and laser treatment of degenerative cartilage deceases.

Keywords Magnetite · Biocompatible nanoparticles · Cartilage degradation · Polysaccharides · Nanomedicine

Electronic supplementary material The online version of this article (doi:10.1007/s11051-013-2092-5) contains supplementary material, which is available to authorized users.

Y. M. Soshnikova (✉) · O. I. Baum · E. N. Sobol
Institute on Laser & Information Technologies, Russian Academy of Sciences, Troitsk 142190, Russia
e-mail: yuliasoshnikova@gmail.com

Y. M. Soshnikova · M. V. Obrezkova · V. V. Lunin
Department of Chemistry, Lomonosov Moscow State University, Moscow 119992, Russia

S. G. Roman · N. A. Chebotareva
A.N. Bach Institute of Biochemistry, Moscow 119071, Russia

R. B. Gillis · S. E. Harding
National Centre for Macromolecular Hydrodynamics, University of Nottingham, Nottingham LE12 5RD, UK

Introduction

There has recently been a significant growth of interest in the use of nanoparticles (NPs) in diagnostics and medicine (Hazer et al. 2012a, b). For example, metal oxide NPs are currently used as contrast agents in magnetic resonance imaging (Chen et al. 2012). In optical tomography metal oxide NPs, due to their contrast and stability, are replacing organic fluorescent labels (Xu et al. 2009). New methods for drug delivery (De Jong and Borm 2008) and cancer hyperthermia (Khandhar et al. 2011) based on biocompatible metal oxide NPs are also being developed. The use of NP additives as adsorbers of laser irradiation is another possible application of NPs in laser medicine (Popov et al. 2007). Such application allows to reduce the laser power requirements and to concentrate energy in the damaged areas where the NPs are distributed, thus lowering the exposure of healthy areas of tissue to laser damage.

Biocompatible iron oxide NPs are of great interest due to their ability of magnetically controlled transportation and surface modification by polymers and surfactants (Mornet et al. 2004; Estevanato et al. 2012). The most common magnetic agents are magnetite Fe_3O_4 (Majewski and Thierry 2008) and maghemite Fe_2O_3 (Mornet et al. 2002). Other magnetic agents are also utilized—e.g., alloys of iron with cobalt (Chaubey et al. 2007), nickel (Chen et al. 2010), and platinum (Lai et al. 2012).

Other applications for magnetic NPs include laser reshaping and treatment of cartilage. Cartilage degradations arise in small localized areas and are difficult to identify in their early stages. They can be medically diagnosed only when the size of the damaged area is relatively large ($\sim$1 mm in diameter) (Shyu et al. 2009; Stolz et al. 2004, 2009; Crocketta et al. 2005). Consequently, it would be useful to develop a method for the diagnosis of the extent of cartilage degradation in the early stages when the defects are small, i.e., of micron size. Unfortunately, a well known tendency of magnetic NPs to form aggregates or agglomerates impedes their medical application (Lim and Feng 2012). However, the surface modification of magnetic NPs by different organic substances can significantly improve the stability of their dispersions. In the case of magnetite NPs, these modifications can also help to prevent oxidation reactions (Kim et al. 2001; Lin et al. 2010; Sun et al. 2009). Polysaccharides derived from natural raw materials are particularly promising stabilizers (Daniel-da-Silva and Trindade 2011). These substances improve the biocompatibility of magnetic NPs by providing a surrounding polymer matrix. They also result in additional biofunctionality due to bonding of their functional groups to macromolecular tissue.

In the present study we use the potato starch as a known stabilizer for the modification of magnetite NPs. Our complex of research methods provides information about the agglomeration properties and especially about the thermal and storage stability—something that is not fully described in the literature but is essential for medical application of the NPs. Appropriate preparation conditions for creation of non-volatile and thermally stable aqueous dispersions of magnetite NPs are established. We show that synthesized magnetite NPs penetrate into damaged and healthy cartilage and that the size of impregnated particles indicates the degree of cartilage degradation.

Experimental

Synthesis of magnetite NPs

All chemicals were of analytical grade. In all experiments water was deionized with an Easy-Pure II RF system (Barnstead). The following reagents were used: ferrous chloride tetrahydrate $FeCl_2{\cdot}4H_2O$ (Sigma), ferric chloride hexahydrate $FeCl_3{\cdot}6H_2O$ (Sigma), ammonia aqueous solution NH_3 25 % (ChemReagent), and potato starch (ChemReagent).

The reaction was carried out according to the following scheme:

$$2Fe^{3+} + Fe^{2+} + 8OH^- = Fe_3O_4 \downarrow + 4H_2O$$

Firstly, 0.05 M $FeCl_3$ and 0.025 M $FeCl_2$ were dissolved in deionized and deoxygenized water in an argon atmosphere. The solution was separated in 4 portions: 1 was left invariable, in 2; 3; and 4 starch was added to a % mass concentration 0.1, 0.5, and 1.0. The mixtures were heated to 90 °C and ammonia was added under vigorous stirring until the formation of a stable black precipitate. The final pH was 12. Solutions were stirred for 15 min and left for 1 h in an inert atmosphere. Then the magnetite precipitate was separated and washed with water several times. After drying in an inert atmosphere at room temperature magnetite was dispersed in water and large particles were removed by centrifugation.

Secondly, four dispersions of magnetite were synthesized according to the previous technique with one difference: starch was added in portions two, three, and four immediately after formation of the precipitate.

Dynamic light scattering (DLS)

DLS measurements were performed on a Photocor (Photocor Instruments Inc., USA) laser light scattering photometer with a He–Ne laser (power 10 mW, $\lambda = 632.8$ nm) (Coherent, CIIIA, model 31-2082) and a Zetasizer Nano ZS (Malvern, Great Britain). DynalS software (Alango, Israel) was used to analyze the DLS data in terms of hydrodynamic radii (R_h) and polydispersity indexes (PIs) of the particles.

Analytical ultracentrifugation (AUC)

AUC was performed on a Beckman (Palo Alto, USA) Model E ultracentrifuge Spinco (Beckman) equipped

with absorbance optics, a photoelectric scanner, a monochromator, and an online computer. The rotor speed was 24,000 rpm. Sedimentation velocity experiments were carried out at 20 °C. The sedimentation coefficients were estimated from the differential sedimentation coefficient distribution [$c(s)$ vs. s] using the SEDFIT program (Lebowitz et al. 2002). The average sedimentation coefficients of particular species were obtained by integrating distributions $c(s)$.

Asymmetrical flow field flow fractionation (A4F)

A4F experiments were performed on an Eclipse 3 separation system (Wyatt Technology Corporation, USA) based on an Agilent HPLC pump (Agilent Technologies, USA) at room temperature (27 °C). A 21.4-cm channel with a 350-mm channel spacer and ultrafiltration membrane made of regenerated cellulose with a 5-kDa molecular weight cutoff (Wyatt Technology Corporation, USA) was used. The ASTRA software, version 5.3.4 (Wyatt Technology Corporation, USA) was used to yield the final profiles.

Transmission electron microscopy (TEM)

For TEM analysis magnetite NPs samples were applied to copper grids 3 mm in diameter covered with ultrathin polymer layer. The experiment was performed on JEOL JEM-2000 FXII microscope (JEOL Ltd., Japan) operating at 200 kV. For tissue TEM analysis specimens of cartilage were fixed and dried in epoxy resin, cut on microtome to 100 nm slices, and analyzed at 200 kV.

Experiments on biological tissue

Porcine costal cartilage was separated from the perichondrium and cut with a surgical scalpel to slices of 3.0 mm thickness. Three series of biological samples were prepared. For the first series the cartilage slices were irradiated by an erbium fiber laser (Arcuo Medical, Inc., Los Altos, CA, USA) according to the previously developed technique described in Baum et al. (2011) to simulate the damaged cartilage. The samples from the second cartilage series were left intact. Half of the specimens of both series was incubated in magnetite NP dispersion containing 0.5 % mass of starch for 24 h. Then the specimens were extracted and washed with sterile saline solution. Another half was left without incubation. For TEM analysis specimens of cartilage that had been previously incubated with NPs were fixed and dried in epoxy resin, cut on microtome to 200 nm slices, applied to a copper grid, and then analyzed at 200 kV. Atomic force microscopy (AFM) experiments on non-incubated cartilage were carried out using a scanning tunnel microscope Nanoscope IIIa (Digital Instruments, Santa Barbara, USA). The tissue specimens were cut on a microtome to 20 μm slices and applied to glass substrates for AFM analysis. Height profiles were obtained on air in tapping mode, scanning rate 1.5 Hz, and resonant frequency 2.0 V. The collected data were analyzed using Gwyddion 2.03 software (courtesy of David Nečas and Petr Klapetek).

Results and discussion

DLS allows to evaluate the sizes of synthesized magnetite NPs via measurements of the (z-average) translational diffusion coefficient (D) distribution. The hydrodynamic radii, R_h, of equivalent spherically shaped particles were calculated from the diffusion coefficients by the Stokes–Einstein equation: $D = k_B T/6\pi\eta R_h$, where k_B is the Boltzmann constant, T is the absolute temperature, and η is the viscosity of the dispersing medium. While such calculation is correct for spherical and homogeneous particles, in other cases it gives only an estimate of hydrodynamic radii. Therefore, we use the term "apparent" for referring the Stokes–Einstein radii determined by DLS.

Figure 1 presents size distribution of aqueous dispersions of non-stabilized magnetite NPs. Conspicuously the system is very polydisperse with hydrodynamic radii values in the range of (150–850) nm and an apparent average $<R_h>$ value of 330 ± 10 nm (mean $\pm$ SD, $n = 60$).

Estimates for the size distributions (as estimated by DLS) of magnetite NPs dispersions synthesized in the presence of increasing amounts of starch are presented in Fig. 2. Average values of hydrodynamic radii and PIs for dispersions of NPS synthesized in the presence of 0.1, 0.5, and 1.0 % of starch are 85 ± 6 nm (PI $= 0.44 \pm 0.04$), 48 ± 1 nm (PI $= 0.52 \pm 0.04$), and 33 ± 1 nm (PI $= 0.45 \pm 0.03$), respectively. Thus, increasing the amount of starch from 0.1 to 1 mass% results in the decrease in the average size of the NPs.

We also verified whether the moment of the starch addition during the synthetic procedure of magnetite NPs influences the size of obtained NPs. Figure 3 shows the size distribution of magnetite NPs dispersion modified with starch after formation of the magnetite. The apparent R_h and PI values are 110 ± 1 nm and 0.72 ± 0.07, respectively.

Comparative DLS data for all magnetite dispersions are presented in Table 1.

The observed data show that the addition of starch to the magnetite dispersions leads to a shift of the distribution toward the smaller particles (<100 nm) although the "tail" of the distribution still shows large particles of up to 1,000 nm (Figs. 1, 3). The presence of starch at the moment of precipitation dramatically changes the final distribution of magnetite NPs (Fig. 2). The average hydrodynamic radius in such system is at least two times less than that for post-stabilized system (Table 1). Thus, the presence of starch at the moment of synthesis influences the process of particles growth and reduces the rate of formation of agglomerates. The increase of starch concentration in the system results in a corresponding decrease of the average radius value and makes the distribution narrower.

We should note that DLS is a more sensitive probe for larger particles (>10 nm), whereas the analytical ultracentrifuge provides a more sensitive probe for smaller particles (see, for example, Philo 2006). Therefore, the dispersions of Fe_3O_4 NPs synthesized

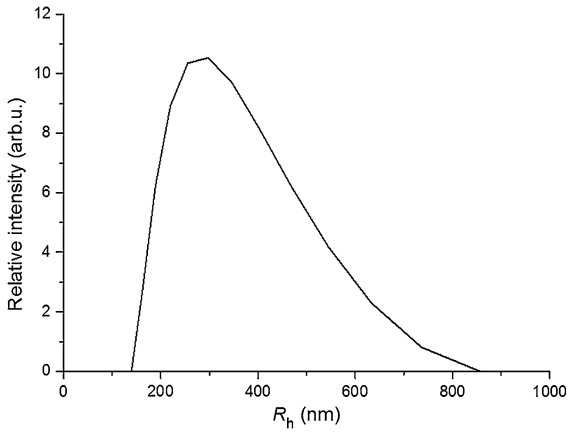

Fig. 1 Size distribution for the aqueous dispersion of non-stabilized Fe_3O_4 NPs dispersion determined by DLS at 25 °C

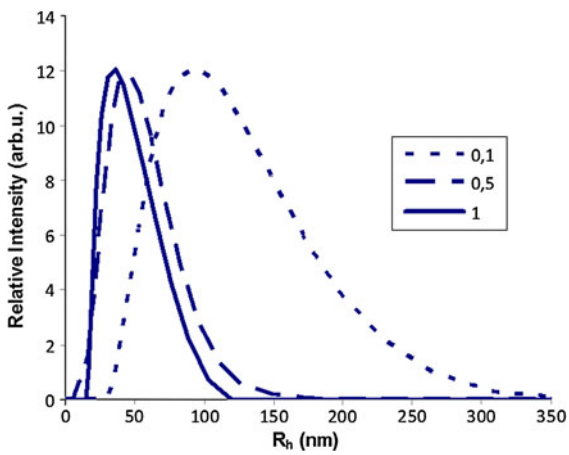

Fig. 2 Size distributions for the aqueous dispersions of Fe_3O_4 NPs synthesized in presence of 0.1, 0.5, and 1 % of starch determined by DLS at 25 °C

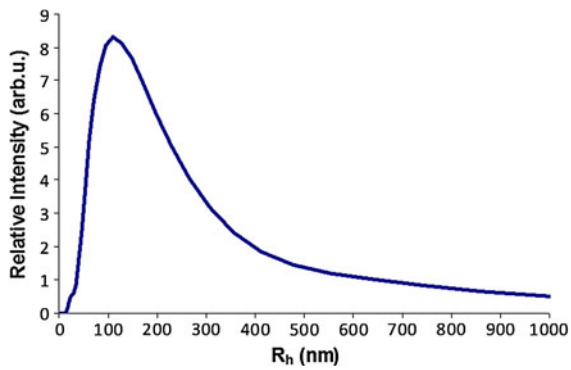

Fig. 3 Size distribution for the aqueous dispersion of Fe_3O_4 NPs modified with 0.5 % of starch after precipitation of magnetite determined by DLS at 25 °C

Table 1 Average hydrodynamic radii of Fe_3O_4 NPs in aqueous dispersions

Starch concentration used in the synthesis of Fe_3O_4 NPs (%)	$<R_h>$ (nm)	PI
0.0	274 ± 7	Not available, highly polydisperse system
0.1	85 ± 6	0.44 ± 0.04
0.5	48 ± 1	0.52 ± 0.04
0.5 (starch was added after the formation of the precipitate)	110 ± 1	0.72 ± 0.07
1.0	33 ± 1	0.45 ± 0.03

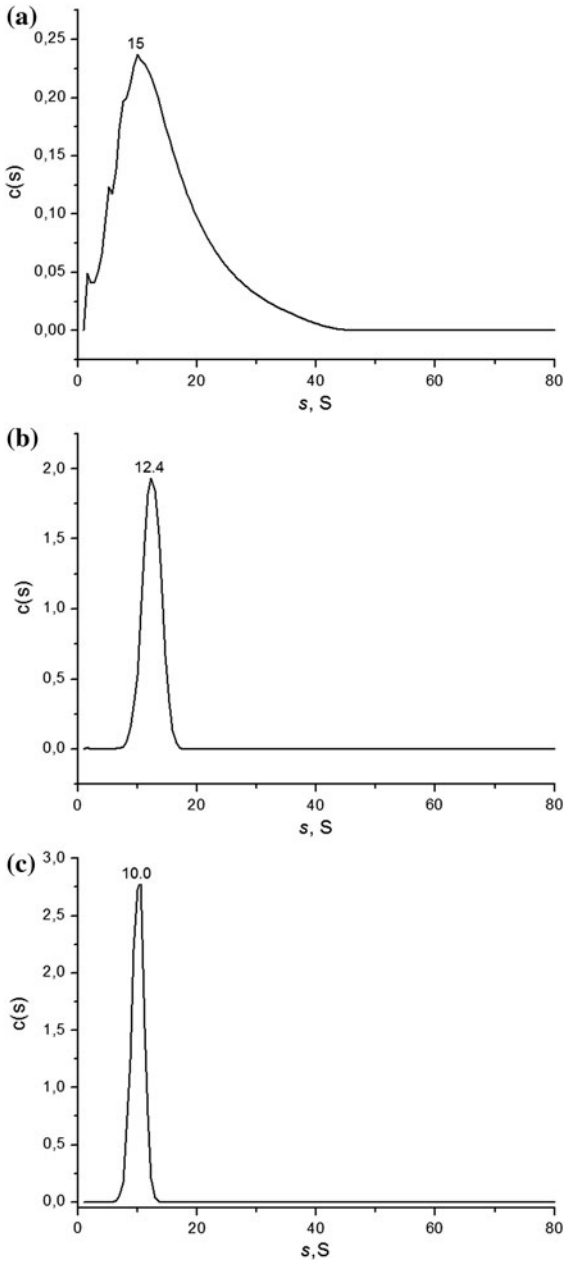

Fig. 4 Differential distributions of sedimentation coefficients $c(s)$ versus s for Fe_3O_4 NPs synthesized in the presence of **a** 0.1, **b** 0.5, and **c** 1.0 % of starch correspondingly (20 °C, rotor speed was 24,000 rpm)

in the presence of varying concentrations of starch were also carried out by means of AUC to analyze very small fractions. Fe_3O_4 NPs aqueous solutions were preliminarily centrifuged in the AUC for 15 min at 5,000 rpm/min (=1,800 g) to remove very large particles—the remaining solutions that contained about 88–90 % of initial Fe_3O_4 mass (determined by optical density analysis at $\lambda = 307$ nm after separation of large particles) were then studied. The distributions of sedimentation coefficient of the starch-modified magnetite NPs dispersions are presented in Fig. 4. The average sedimentation coefficients values (s_{av}) in dispersions of NPs synthesized in the presence of 0.1, 0.5, and 1.0 % of starch are 15.0, 12.4, and 10.0 S, respectively, and the average Stokes radii were estimated to be 4.9, 4.8, and 3.7 nm, respectively. Though the average Stokes radii values are close, one can see that as starch concentration increases, the distribution $c(s)$ narrows. Comparison of Fig. 4a, c demonstrates that the $c(s)$ distribution for NPs dispersion modified with 1 % of starch does not include particles with sedimentation coefficients in the range of 20–50 S whereas the $c(s)$ distribution for NPs dispersion modified with 0.1 % of starch does. Therefore, we can reasonably infer that the sedimentation velocity data confirm the stability of small and uniform particles with the increase of starch concentration up until 1 %.

For impregnation into cartilage we selected the Fe_3O_4 NP dispersion modified with 0.5 % of starch. The data that follow refer to this preparation.

A4F represents a powerful method for the determination of particle size and molar mass distributions, detection and characterization of aggregates in solution, and characterization of polymer branching (Podzimek 2011). However, because of the uncertainty about Fe_3O_4 concentration and specific refractive index increment value of Fe_3O_4 NPs modified with 0.5 % starch solution, we used only the DLS signal for subsequent analysis in the present investigation. A4F separated synthesized magnetite particles by hydrodynamic size while DLS allowed direct measurement of R_h of the particles. Figure 5 shows the elution profile of Fe_3O_4 NPs aqueous dispersion modified with 0.5 % of starch registered as a time-dependence of DLS detector signal. As one can see, the sample profile runs a broad range of elution times indicating the polydispersity of the sizes of synthesized magnetite particles. However, the major fraction of particles has the R_h values in the range of 40–50 nm as evidenced by the values of the R_h calculated from the DLS data. The mean R_h value for the peak equals to 46.5 ± 0.3 nm (see inset in Fig. 5). Particles with R_h values higher than 50 nm are also detected in the

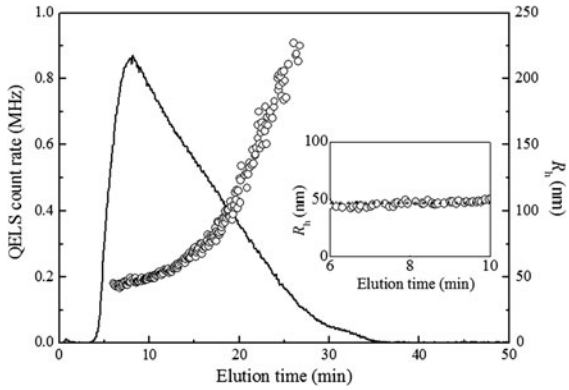

Fig. 5 A4F data for Fe_3O_4 NPs dispersion synthesized in the presence of 0.5 % of starch

solution but their contribution to the overall signal decreases markedly with size. Thus, these data are in good agreement with the DLS data above.

The magnetite NPs and the agglomerates were visualized using TEM combined with electron diffraction measurements. The TEM data provide an evaluation of the form and size of the particles and an assessment of their crystalline structure. Figure 6a, b presents the TEM images for both the non-stabilized and the starch (0.5 %) stabilized magnetite dispersions respectively.

Figure 6a shows large agglomerates (more than 100 nm) constructed from domains about 20 nm. Figure 6b presents NPs of 5–20 nm in diameter and also agglomerates of up to 100–200 nm. These findings correspond with sedimentation velocity and DLS data. The observed differences in average particle sizes provided by DLS and TEM can be explained as follows. DLS is very sensitive for the large particles. The intensity of the DLS signal depends on the size of a scattering center as $I \sim r^6$,

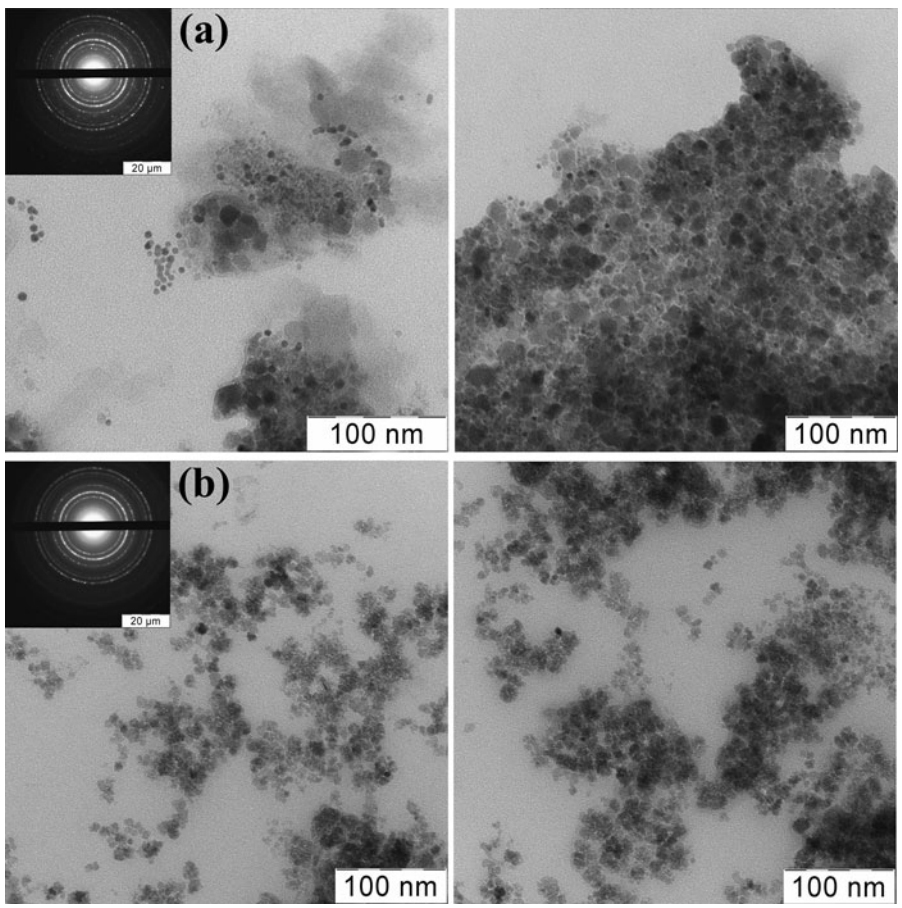

Fig. 6 TEM images of Fe_3O_4 dispersions **a** non-stabilized, **b** synthesized in presence of 0.5 % starch. The *inserts* show the diffraction patterns of the samples

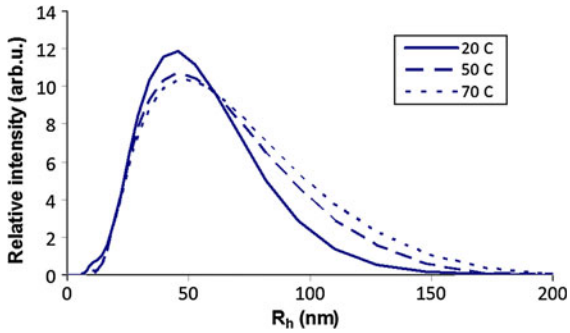

Fig. 7 Temperature-dependent size dynamics of Fe_3O_4 dispersion synthesized in presence of 0.5 % starch

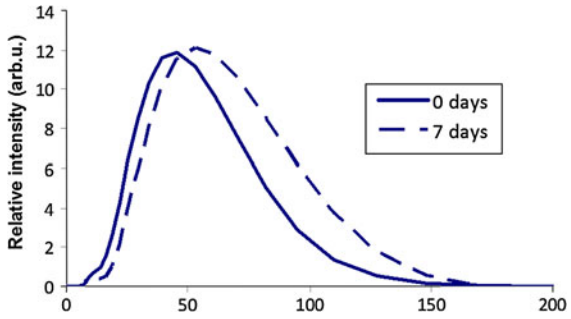

Fig. 8 Time-dependent size dynamics of Fe_3O_4 dispersion synthesized in the presence of 0.5 % of starch

and the total intensity of large particles is higher even if their cumulative contribution to the whole number of particles is not so high. Thus, the average value of DLS distribution is always shifted to large sizes. TEM images demonstrate that there are a lot of small particles with diameters far smaller than 50 nm and also their agglomerates with diameters of about 100 nm. The total amount of agglomerates is not high as it is shown by TEM and AFM analysis but it can be enough to impact the DLS result and shift the apparent hydrodynamic radius to larger values. However, both methods confirm the tendency that the degree of agglomeration of the NPs can be decreased by starch stabilization. In comparison to the non-stabilized magnetite the particles in the starch dispersions are more uniformly distributed and the contribution of small particles appears to be higher.

The diffraction pattern inserts to Fig. 6a, b confirm the highly crystalline structure of synthesized particles of both types.

Figure 7 shows stability results derived from DLS measurements under changing temperature from 20 to 70 °C. This temperature range is determined according to the conditions of therapeutic laser cartilage treatment (Baum et al. 2011). As one can see from Fig. 7, the average hydrodynamic radius of the particles has negligible changes as temperature increases. This result approves the ability of such systems of NPs to be used in the laser therapy of biological tissues when the temperature of operating tissue surface does not exceed 70 °C.

The time-dependent stability of Fe_3O_4 NPs was also studied by DLS (Fig. 8). In 7 days after synthesis and storage at room temperature in inert atmosphere the average hydrodynamic radius of Fe_3O_4 NPs changes insignificantly and is 52 ± 1 nm in comparison to 48 ± 1 nm for the just prepared dispersion. This increase does not affect the whole distribution and the properties of magnetite dispersion do not change within this time interval. It is worth noting that the time stability is important for NPs storage and subsequent medical application.

Both healthy and damaged types of cartilage were tested in NPs impregnation experiment. The tissue defects that simulate the early degradation stage of cartilage were created by fine laser impact according to the previously developed technique (Baum et al. 2011). For impregnation testing we used the 0.5 % starch-modified Fe_3O_4 dispersion. Figure 9a, b present the AFM images of damaged and healthy cartilage, respectively. One can see that in Fig. 9a the collagen network is mostly broken and disorganized. Such disorganization is postulated to be the initial stage of cartilage degradation that causes arthritis (Stolz et al. 2009). It can be characterized as the structure that contains nano- and micro-pores and defects depending on the stage of degradation. Healthy cartilage (Fig. 9b) demonstrates that the well-organized collagen network and the fibrils are clearly intact. The results of polydisperse NPs impregnation into damaged and healthy cartilage are shown in Fig. 9c, d, respectively. The concentration of NPs impregnated into damaged cartilage turns out to be comparatively high and the range of examined diameters is 5–100 nm. The large NPs and their agglomerates from 50 to 100 nm are mostly found in the surface layer of damaged cartilage (no more than 200 nm in depth). It demonstrates that the cartilage is at an early stage of degradation and contains pores and channels of structure of about 100–200 nm in diameter. The presence of large particles deeper than 200 nm in

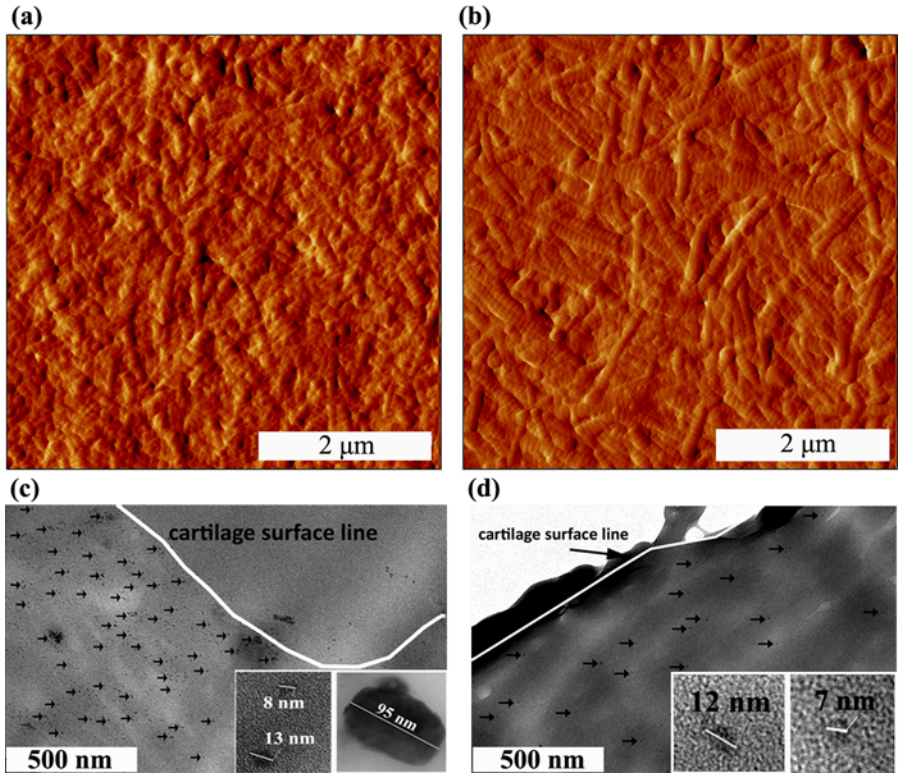

Fig. 9 Surface imaging of different types of cartilage and magnetite NPs impregnation testing. **a** AFM image of cartilage surface with laser-simulated early stage defects. The collagen network appears to be disorganized. **b** AFM image of healthy cartilage surface. Collagen fibrils are intact. Their periodic structure is observed. **c** TEM image of damaged cartilage impregnated with magnetite NPs. The concentration is comparatively high; the range of visible diameters is 5–100 nm. **d** TEM image of healthy cartilage impregnated with magnetite NPs. The concentration is comparatively low; the range of visible diameters is 5–15 nm

structure can be explained by the concentration of small NPs in growing defects of the damaged tissue. The healthy cartilage (Fig. 9d) contains only small particles of about 5–15 nm in diameter and their concentration compared to the ones impregnated in damaged cartilage is lower. The obtained data correspond to the previously examined types of damaged and healthy cartilage in (Sobol et al. 2000) where the porous structure of damaged cartilage was evaluated. The analysis of Fig. 9c and d shows that the use of the polydisperse NPs system provides the visualization of cartilage pores and channels structure. The size and concentration of impregnated NPs depend on the degree of tissue degradation. Based on the obtained results we can suggest that utilization of polydisperse NPs system (up to 100 nm) will allow to investigate structure channels distribution of cartilage and its dependence on tissue type (healthy or damaged) and on the conditions of preliminary processing (irradiation in different modes). Thus, impregnation of NPs into cartilage creates new condition-dependent possibilities for research of tissue structure.

Conclusions

Polydisperse magnetite aqueous dispersions have been synthesized. An analytical study of their distribution revealed the simultaneous presence of small particles (up to 10 nm in diameter) and large agglomerates of about 1 μm and more. It has been shown that starch-modified dispersions are more stable with a narrower distribution; the contribution of small particles (up to 100 nm) prevails. Increase of the amount of starch from 0.1 to 1 mass% results in the decrease in average size of the particles. Presence of starch at the moment of chemical synthesis of magnetite prevents the forming particles from instant agglomeration.

Starch-modified magnetite dispersions are stable during a temperature increase from 20 to 70 °C. This appears to vindicate the ability of such systems to be used in the laser therapy of biological tissues when the temperature of operating tissue surface does not exceed 70 °C. We also have studied time-dependent stability of the systems. An insignificant increase of the average size is indicated in 7 days after the preparation. This increase does not affect the whole distribution and the properties of the magnetite dispersion do not appear to change. This type of stability is important for the storage of NPs and subsequent medical application, a topic worthy of further consideration. Cartilage structural features are responsible for the ability of NPs application in the control of tissue irradiation. It has been recently shown that cartilage has porous structure with the size of the channels depending on the tissue type, its age, damage degree, and also preliminary operations (including laser irradiation). Structure pores and channels provide liquid transfer and cell nutrition throughout the tissue, as cartilage does not have blood vessels. Thus, the structure of cartilage allows impregnation of NPs through its pores and channels. As we have shown in the present study, magnetite NPs about 10 nm in diameter penetrate into healthy cartilage, and this NP size corresponds to the same pores distribution. Cartilage degradation appears in more than 1 μm cracks, and this allows penetration of large particles. Therefore, polydisperse magnetite dispersion can be used to determine micro defects of tissue. Medical laser impact of the damaged cartilage structure impregnated with absorbing NPs will allow to perform local and dedicated treatment with lower laser power. Magnetite NPs appear to be a promising proposition for use in the diagnostics and optimization of medical laser treatment of cartilage.

Acknowledgments The authors thank Richard Thelen for technical assistance in AFM investigations. The work was supported by Russian Foundation of Basic Research Grants 11-02-92614, 12-08-13166, and 12-02-91326. This work was partly carried out with the support of the Karlsruhe Nano Micro Facility (KNMF, www.kit.edu/knmf), a Helmholtz Research Infrastructure at Karlsruhe Institute of Technology (KIT, www.kit.edu).

References

Baum OI, Soshnikova YuM, Sobol EN, Korneychuk AYa, Obrezkova MV, Svistushkin VM, Timofeeva OK, Lunin VV (2011) Laser reshaping of costal cartilage for transplantation. Lasers Surg Med 43:511–515

Chaubey GS, Barcena C, Poudyal N, Rong CJ (2007) Synthesis and stabilization of FeCo nanoparticles. Am Chem Soc 129:7214–7215

Chen Y, She H, Luo X, Yue GH, Mi WB, Bai HL, Peng DL (2010) Chemical synthesis of monodisperse Fe–Ni nanoparticles via a diffusion-based approach. J Nanosci Nanotechnol 10(5):3053–3059

Chen J, Wang F, Zhang Y, Jin X, Zhang L (2012) In vivo tracking of superparamagnetic iron oxide nanoparticle labeled chondrocytes in large animal model. Ann Biomed Eng 40(12):2568–2578

Crocketta R, Roosa S, Rossbacha P, Dorab C, Bornb W, Troxlerc H (2005) Imaging of the surface of human and bovine articular cartilage with ESEM and AFM. Tribol Lett 19(4):311–317

Daniel-da-Silva AL, Trindade T (2011) Biofunctional composites of polysaccharides containing inorganic nanoparticles. In: Abbass Hashim (ed) Advances in nanocomposite technology. InTech, Sheffield, UK, pp 275–298. ISBN: 978-953-307-347-7

De Jong WH, Borm PJA (2008) Drug delivery and nanoparticles: applications and hazards. Int J Nanomed 3(2):133–149

Estevanato LL, Lacava LM, Carvalho LC, Azevedo RB, Silva OJ (2012) Long-term biodistribution and biocompatibility investigation of dextran-coated magnetite nanoparticle using mice as the animal model. Biomed Nanotechnol 8(2):301–308

Hazer DB, Kiliçay E, Hazer B (2012a) Poly(3-hydroxyalkanoate)s: diversification and biomedical applications: a state of the art review. Math Sci Eng 32:637–647

Hazer DB, Mut M, Dinçer N, Sarıbas Z, Hazer B, Özgen T (2012b) The efficacy of silver-embedded polypropylene-grafted glycol-coated ventricular catheters on prevention of shunt catheter in rats. Childs Nerv Syst 28:839–846

Khandhar AP, Ferguson RM, Krishnana KM (2011) Monodispersed magnetite nanoparticles optimized for magnetic fluidhyperthermia: implications in biological systems. J Appl Phys 109:07B310–07B3103

Kim DK, Voit W, Zapka W, Bjelke B (2001) Biomedical application of ferrofluids containing magnetite nanoparticles. Mater Res Soc Symp Proc 676:Y8.32.1–Y8.32.6

Lai SM, Tsai TYu, Hsu ChY (2012) Bifunctional silica-coated superparamagnetic FePt nanoparticles for fluorescence/MR dual imaging. J Nanomater. doi:10.1155/2012/631584

Lebowitz J, Lewis MS, Schuck P (2002) Modern analytical ultracentrifugation in protein science: a tutorial review. Protein Sci 11:2067–2079

Lim EW, Feng R (2012) Agglomeration of magnetic nanoparticles. J Chem Phys 136(12):124109. doi:10.1063/1.3697865

Lin MM, Li Sh, Kim HH, Kim HJ (2010) Complete separation of magnetic nanoparticles via chemical cleavage of dextran by ethylenediamine for intracellular uptake. Mater Chem 20:444–447

Majewski P, Thierry B (2008) Functionalized magnetite nanoparticles—synthesis, properties, and bioapplications, particulate systems in nano- and biotechnologies. CRC Press\University of Florida, Boca Raton\Gainesville

Mornet S, Grasset F, Portier J, Duguet E (2002) Maghemite@silica nanoparticles for biological applications. Eur Cells Mater 3:110–113

Mornet S, Vasseur S, Grasset F, Duguet EJ (2004) Magnetic nanoparticle design for medical diagnosis and therapy. Mater Chem 14:2161–2175

Philo JS (2006) Is any measurement method optimal for all aggregate sizes and types? AAPS J 8(3):E564–E571

Podzimek S (2011) Light scattering, size exclusion chromatography and asymmetric flow field flow fractionation. Wiley, Hoboken

Popov AP, Priezzhev AV, Myllylä R (2007) Optimal sizes of gold nanoparticles for laser treatment of tumors. Proc SPIE 6534:65343K-1–65343K-5

Shyu JJ, Chan CH, Hsiung MW, Yang PN, Chen HW (2009) Diagnosis of articular cartilage damage by polarization sensitive optical coherence tomography and the extracted optical properties. Prog Electromagn Res PIER 91: 365–376

Sobol E, Sviridov A, Omelchenko A, Bagratashvili V, Kitai M, Harding SE (2000) Laser reshaping of cartilage. Biotechnol Genet Eng Rev 17:553–578

Stolz M, Raiteri R, Daniels AU, VanLandingham MR (2004) Dynamic elastic modulus of porcine articular cartilage determined at two different levels of tissue organization by indentation-type atomic force microscopy. Biophys J 86:3269–3283

Stolz M, Gottardi R, Raiteri R, Miot S, Martin I (2009) Early detection of aging cartilage and osteoarthritis in mice and patient samples using atomic force microscopy. Nat Nanotechnol 4:186–192

Sun X, Zheng Ch, Zhang F, YaJ Yang (2009) Size-controlled synthesis of magnetite (Fe_3O_4) nanoparticles coated with glucose and gluconic acid from a single Fe(III) precursor by a sucrose bifunctional hydrothermal method. J Phys Chem 113(36):16002–16008

Xu CT, Axelsson J, Andersson-Engels S (2009) Fluorescence diffuse optical tomography using upconverting nanoparticles. Appl Phys Lett 94:251107. doi:10.1063/1.3156857